# Codependencies of mTORC1 signaling and endolysosomal actin structures

Amulya Priya, Sandra Antoine-Bally, Anne-Sophie Macé, Pedro Monteiro, Valentin Sabatet, David Remy, Florent Dingli, Damarys Loew, Constantinos Demetriades, Alexis Gautreau, et al.

DEVELOPMENTAL BIOLOGY

# Codependencies of mTORC1 signaling and endolysosomal actin structures

**Amulya Priya[1]†, Sandra Antoine-Bally[1], Anne-Sophie Macé[2], Pedro Monteiro[1], Valentin Sabatet[3], David Remy[1], Florent Dingli[3], Damarys Loew[3], Constantinos Demetriades[4,5], Alexis M. Gautreau[6], Philippe Chavrier[1]***



**The mechanistic target of rapamycin complex 1 (mTORC1) is part of the amino acid sensing machinery that becomes activated on the endolysosomal surface in response to nutrient cues. Branched actin generated by WASH and Arp2/3 complexes defines endolysosomal microdomains. Here, we find mTORC1 components in close proximity to endolysosomal actin microdomains. We investigated for interactors of the mTORC1 lysosomal tether, RAGC, by proteomics and identified multiple actin filament capping proteins and their modulators. Perturbation of RAGC function affected the size of endolysosomal actin, consistent with a regulation of actin filament capping by RAGC. Reciprocally, the pharmacological inhibition of actin polymerization or alteration of endolysosomal actin obtained upon silencing of WASH or Arp2/3 complexes impaired mTORC1 activity. Mechanistically, we show that actin is required for proper association of RAGC and mTOR with endolysosomes. This study reveals an unprecedented interplay between actin and mTORC1 signaling on the endolysosomal system.**

## INTRODUCTION

Adaptation of cell growth and metabolism to nutritional and environmental cues are controlled by the serine/threonine (Ser/Thr) mechanistic target of rapamycin (mTOR) kinase (*1*). mTOR exists in two multisubunit protein complexes, mTORC1 and mTORC2, with distinct cellular functions and localization. Plasma membrane–associated mTORC2 regulates prosurvival pathways and cortical cell cytoskeleton organization in relation with phosphoinositide 3-kinase signaling through protein kinase C and AKT kinase control (*1*). mTORC1, which controls cell responses to nutrients, associates with the surface of lysosomes under amino acid replete conditions by interacting with active RAG heterodimers ($RAGA^{GTP}$ or $RAGB^{GTP}$ bound to $RAGC^{GDP}$ or $RAGD^{GDP}$) (*2*–*4*). The LAMTOR complex (also known as Ragulator, composed by LAMTOR1/p18, LAMTOR2/p14, LAMTOR3/MP1, LAMTOR4/p10, and LAMTOR5/HBXIP) (*5*) acts as a RAGA/B guanine nucleotide exchange factor (GEF) in a mechanism involving the lysosomal vacuolar adenosine triphosphatase (v-ATPase) and the amino acid transporter SLC38A9 (*6*–*10*). In addition, the guanosine triphosphatase (GTPase) activating protein (GAP), folliculin, maintains RAGC (and RAGD) in the guanosine diphosphate (GDP)–bound state (*11*). $RHEB^{GTP}$ activates mTORC1 primarily on the lysosomal surface, which can then phosphorylate key factors of protein translation, including S6K (P70 S6 kinase 1) and 4E-BP1 (eukaryotic initiation factor 4E binding protein 1). At the same time, phosphorylation by mTORC1 inhibits the autophagy initiator, ULK1, and the transcription factor EB (TFEB) (*3*). In the absence of amino acids, the Rag GAP complex GATOR1 switches RAGA/B in the Rag dimer to a GDP-bound conformation, which promotes recruitment of the tuberous sclerosis complex (TSC) RHEB-GAP complex, RHEB inactivation, and release of mTORC1 from the lysosomal surface (*2*, *3*, *12*).

Endosomal membranes are the assembly sites for small (submicrometric) puncta of branched actin filaments protruding out of the endosome surface (*13*–*15*). Polymerization of branched actin filaments on endosomes is controlled by the Wiskott-Aldrich syndrome protein and scar homolog (WASH) complex (composed of WASHC4 (WASH complex subunit 4, aka SWIP), strumpellin, sequence similarity 21 (FAM21), WASH, and CCDC53 subunits) through activation of the seven-subunit actin-related proteins-2/3 (Arp2/3) actin nucleating complex. Capping protein (CP), composed of a CAPZA/B heterodimer, is critical for the regulation of WASH-Arp2/3 complex-mediated actin structures by terminating actin filament elongation at filament growing ends (*14*–*19*). The FAM21 subunit is critical for endosomal localization of the WASH complex through its high-affinity binding to the VPS35 subunit of the core retromer complex involved in cargo binding and endocytic recycling of various integral membrane proteins (*20*–*24*). Accordingly, loss-of-function studies demonstrated that WASH and F-actin are required for protein sorting and formation of carrier vesicles in the endocytic recycling pathway (*13*, *14*, *20*, *25*–*27*). The key late endosomal/lysosomal protein small GTPase, Rab7, recruits the core retromer complex to endosomes (*28*). In addition, loss of retromer proteins controls the activity and subcompartmentalization of Rab7 (*29*). Further, depletion of retromer proteins alter the subcompartmentalization of Rab7 into Rag-LAMTOR domains, thereby impairing amino acid signaling (*30*). Collectively, these data point to a potential, yet overlooked, link between mTORC1 signaling and endolysosomal Arp2/3 branched actin dynamics.

With that in mind and to better understand mTORC1 signaling on endolysosomes, we investigated a possible interplay between

[1]Institut Curie, CNRS UMR144, PSL Research University, Research Center, Actin and Membrane Dynamics Laboratory, 26 rue d'Ulm, Paris 75248 Cedex 05, France. [2]Institut Curie, PSL Research University, Cell and Tissue Imaging Facility (PICT-IBiSA), 26 rue d'Ulm, Paris 75248 Cedex 05, France. [3]Institut Curie, PSL Research University, CurieCoreTech Mass Spectrometry Proteomics, 26 rue d'Ulm, Paris 75248 Cedex 05, France. [4]Max Planck Institute for Biology of Ageing (MPI-AGE), Cologne, Germany. [5]Cologne Excellence Cluster on Cellular Stress Responses in Aging-Associated Diseases (CECAD), University of Cologne, Cologne, Germany. [6]Laboratoire de Biologie Structurale de la Cellule, CNRS, École Polytechnique, Institut Polytechnique de Paris, Palaiseau, France.
*Corresponding author. Email: philippe.chavrier@curie.fr
†Present address: SickKids Research Institute, The Hospital for Sick Children, 686 Bay Street, Toronto, Ontario M5G 0A4, Canada.

mTORC1 signaling and endolysosomal branched actin. A patchy distribution of several mTORC1 signaling components was observed in the vicinity of WASH-Arp2/3 complexes, F-actin–enriched puncta on endolysosomal compartments. In an interactome analysis, we identified an interaction of RAGC with the actin filament capping machinery and these proteins colocalized on endolysosomes. RAGC depletion enhanced the size of endolysosomal actin puncta, indicative of a regulatory role for RAGC on capping. In addition, various conditions that interfere with endolysosomal branched actin dynamics impaired mTORC1 localization and repressed its activity under nutrient replete conditions. WASH-dependent endolysosomal actin was required for RAGC association to the endolysosomes, while actin disruption led to vesiculation of endolysosomal compartments and dilution of associated signaling components. Together, our data uncover an unsuspected interplay of Arp2/3 branched actin and mTORC1 signaling on endolysosomes.

## RESULTS

### mTORC1 and WASH/F-actin/Arp2/3 complex microdomain organization on endolysosomes

Human breast tumor–derived MDA-MB-231 cells display prominent F-actin and WASH complex (FAM21 subunit)–positive submicrometer size puncta at the surface of juxtanuclear endolysosomes labeled with retromer complex subunit, VPS35, acidotropic dye, LysoTracker, and endolysosomal membrane protein CD63 (Fig. 1A and fig. S1A) (*27*). Similarly, mTOR localization in submicrometric puncta was observed in the vicinity of and partially overlapping with punctate subdomains on endolysosomal membranes enriched for F-actin and Arp2/3 complex subunit, ARPC2 (Fig. 1, A and B, and fig. S1A). RAGC-enriched structures were also visible on endolysosomal compartments overlapping with F-actin- and ARPC2 puncta (Fig. 1C and fig. S1B). In addition, LAMTOR subunits, LAMTOR1 and LAMTOR4, were found in proximity to ARPC2-positive F-actin puncta on endolysosomes (Fig. 1, D and E, and fig. S1, C and D). Together, these data indicate that several mTORC1 signaling components display a microdomain organization overlapping with WASH/Arp2/3 complex branched actin networks on the surface of endolysosomes in MDA-MB-231 cells.

### RAGC interacts with and regulates an endolysosomal actin filament capping machinery

To investigate the molecular environment of the mTORC1-enriched microdomains, we explored the RAGC interactome by endogenous co-immunoprecipitation (co-IP) and quantitative mass spectrometry (MS) analysis. Several proteins identified in the RAGC immunoprecipitates were already known as RAGC interactors including RAGA, RAGB, and LAMTOR1 and could be validated by co-IP and immunoblotting analysis (Fig. 1F). From 3882 quantified proteins in three independent replicates, filtering based on protein quantification from three or more peptides and enrichment of >1.6-fold over control at an adjusted $P$ value < 0.05 identified 189 proteins that comprised the RAGC interactome (Fig. 1F, fig. S1E, and table S1). Several proteins involved in vesicular trafficking and actin cytoskeleton organization were identified including a strong enrichment for barbed end actin filament binding and CPs, CAPZA1/2 and CAPZB, known to interact with FAM21 (Fig. 1F and fig. S1E) (*14*). In addition, the related proteins, CD2-associated protein (CD2AP) and SH3 domain-containing kinase binding protein 1 (SH3KBP1, aka CIN85), known to interact with and modulate CAPZ-binding proteins were identified in the RAGC interactome (*31*) (table S1). Green fluorescent protein (GFP)–tagged CD2AP and CAPZB associated with RAGC and mTOR-positive perinuclear endolysosomes and with endolysosomal branched actin assemblies, which were highly dynamic, based on video microscopy analysis (fig. S1F and movie S1). Knockdown (KD) of all CAPZ family members resulted in the formation of elongated, enlarged F-actin, FAM21-enriched, and cortactin-enriched comets on one side of the endolysosome, fueling vesicular rocketing movement (Fig. 1, G and H and movie S1). Silencing of RAGC also resulted in a clear, although less notable, enlargement of branched actin networks on the endolysosomal surface (Fig. 1, H to J). RAGC activity is controlled by its nucleotide-binding status. The consequences on endolysosomal branched actin networks of overexpression of RAGC mutants locked in the GTP-bound state ($RAGC^{Q120L}$) or with low nucleotide affinity, presumably GDP bound in cells ($RAGC^{S75N}$), were assessed (*7*, *32*). Control MDA-MB-231 cells transfected with an empty FLAG-tag vector showed the typical perinuclear distribution of endolysosomal cortactin-enriched puncta (Fig. 1, K and L). Overexpression of inactive GTP-bound $RAGC^{Q120L}$ did not alter the number of endolysosomal cortactin puncta or the general actin cytoskeleton architecture (Fig. 1, K and L, and fig. S1G). On the contrary, overexpression of active, $RAGC^{S75N}$, resulted in a strong reduction of cytoplasmic cortactin-enriched puncta, while the global organization of the actin cytoskeleton remained unperturbed (Fig. 1, K and L, and fig. S1G). Collectively, these data revealed that a direct interaction between RAGC and the endolysosomal actin capping machinery and RAGC loss of function interferes with endolysosomal actin filament capping, while constitutive activation of RAGC results in a loss of endolysosomal branched actin puncta.

### Endolysosomal branched actin is required for mTORC1 signaling

We next addressed a potential regulation of mTORC1 signaling by endolysosomal F-actin. Cells cultured under nutrient replete conditions were treated with drugs that interfere with actin polymerization in several ways. We used CK-666, a specific inhibitor of the actin nucleating Arp2/3 complex (and structurally related inactive CK-689 compound) (*33*); the barbed end actin filament capping compound, cytochalasin D (CytoD) (*34*); and Latrunculin A (LatA), which sequesters monomeric actin and prevents polymerization (*35*). After a 60-min treatment, Arp2/3 complex inhibitor, CK-666 (200 μM), led to complete disappearance of F-actin puncta on CD63-positive or LysoTracker-labeled endolysosomes, while CytoD (0.5 μM) increased F-actin staining, covering the entire endolysosomal surface in agreement with the reported stabilization of Arp2/3 branched actin networks by CytoD (Fig. 2A and fig. S2A) (*36*). On the basis of fluorescence intensity, there was no notable change in amount of LysoTracker taken up by cells upon treatment with CK-666 or CytoD, implying that endolysosome acidification was not grossly altered under these conditions (fig. S2A). We also assessed the drugs' effect on endolysosome positioning and observed a moderate dispersion and peripheralization of

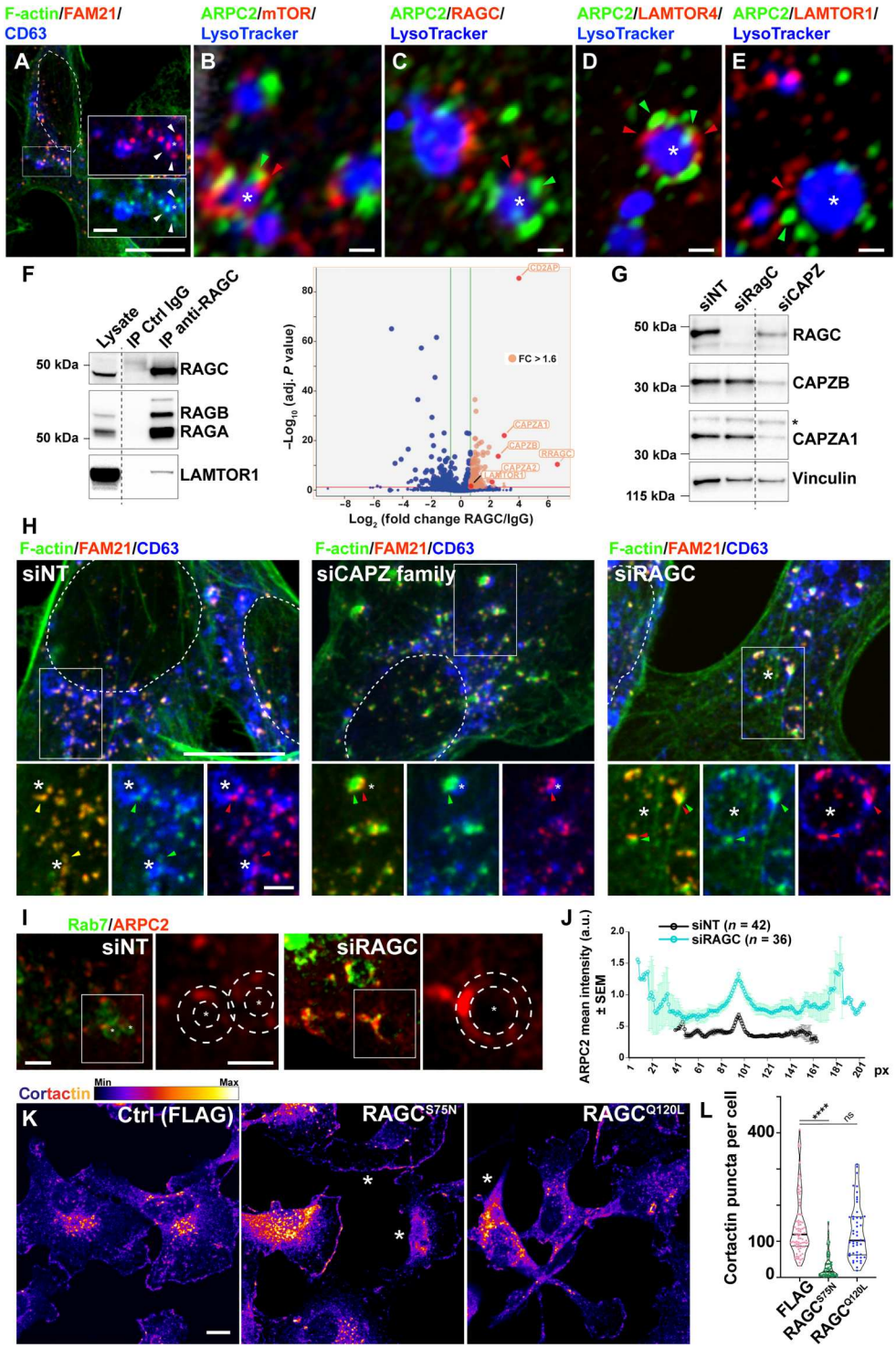


**Fig. 1. mTORC1 signaling components co-localize with branched actin structures on endolysosomes.** (**A** to **E**) MDA-MB-231 cells were fixed and analyzed for indicated mTORC1 components, branched actin network, and endolysosomal markers by immunofluorescence and confocal microscopy. Asterisk denotes endolysosomes, and arrowheads denote microdomains of indicated markers. Nucleus contour is shown with a dashed line (A). In (B) to (E), high-resolution confocal images were acquired on a Airyscan detector-equipped Zeiss confocal microscope. (**F**) Anti-RAGC or control immunoglobulin G (IgG) immunoprecipitates from MDA-MB-231 cell lysates analyzed by immunoblotting with indicated antibodies. Irrelevant lanes were removed, and gel splicing is indicated by dotted line [also in (G)]. Molecular weight markers are in kDa. Right: Volcano plot showing differential anti-RAGC versus Ctrl IgG level ($log_2$, *x* axis) and *P* value ($-log_{10}$, *y* axis) based on quantitative mass spectrometry analysis from three independent experiments. Green line, fold change of 1.6; orange line, *P* value of 0.05. (**G**) Cells knocked down for RAGC or CAPZ proteins (i.e., CAPZA1, CAPZA2, CAPZA3, and CAPZB) by small interfering RNA (siRNA) treatment. Asterisk in the immunoblot points to nonspecific antibody detection. (**H**) Cells knocked down for indicated proteins stained for FAM21 and F-actin puncta and endolysosomal marker, CD63. (**I**) Control or cells silenced for RAGC labeled for Rab7 and Arp2/3 subunit, ARPC2. Dotted lines indicate endolysosomal perimeter region used for linescan analysis. (**J**) Averaged ARPC2 fluorescence profiles ± SEM based on individual line scans recorded along the edge of Rab7-positive endolysosomes and aligned relative to maximum ARPC2 intensity. (**K**) MDA-MB-231 cells expressing FLAG-tagged $RAGC^{Q120L}$ or $RAGC^{S75N}$ or transfected with empty FLAG vector (Ctrl) fixed and labeled for cortactin, FLAG tag, and F-actin (see fig. S1D). Asterisk denotes FLAG-positive cells. (**L**) Number of cytoplasmic cortactin-enriched puncta in indicated cell populations. Scale bars, 10 μm (A, H, and K), 2 μm (B to E and insets), and 1 μm (I). Numerical data and statistical tests are provided in table S5. IP, immunoprecipitation; FC, fold change; a.u., arbitrary units.

Rab7-labeled vesicles upon CK-666 treatment (fig. S2B). Together, these data indicate that acute treatment with actin drugs did not grossly interfere with endolysosome positioning and functionality. In addition, amino acid and serum starvation in Earle's balanced salt solution (EBSS) medium did not visibly affect endolysosomal actin puncta size or numbers, while we noticed an increase in LysoTracker labeling intensity (Fig. 2A and fig. S2A).

We assessed mTORC1 activity by downstream phosphorylation of S6K (on $Thr^{389}$) and 4E-BP1 (on $Ser^{65}$). As expected, mTORC1 activity was strongly repressed upon starvation (Fig. 2A) (*37*). Strikingly, treatment with CK-666 abolished mTORC1 activity, in contrast to inactive CK-689 compound that showed no effect (Fig. 2A). CytoD treatment also reduced mTORC1 activity, although with a slightly reduced efficiency (Fig. 2B). The inhibitory effect of CK-

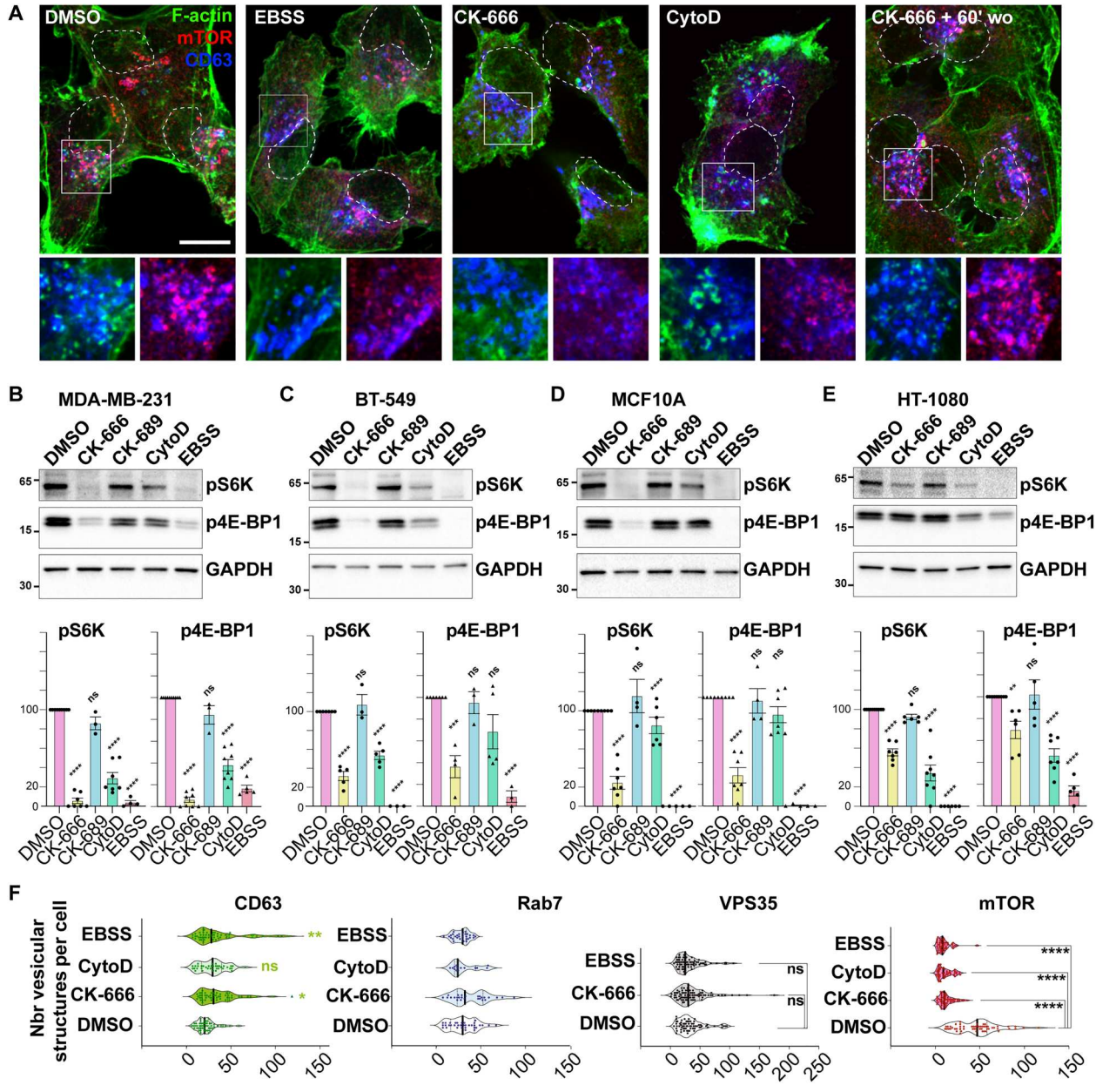


**Fig. 2. Endolysosomal actin dynamics is required for mTORC1 activity.** (**A**) MDA-MB-231 cells with the indicated treatment were fixed and stained for F-actin, mTOR, and CD63. For wash out experiments, cells were treated for 60 min with CK-666, followed by 60 min incubation in the absence of the drug. The nucleus contour is shown with a dashed line. Scale bar, 10 μm. (**B** to **E**) Cells in complete medium were treated with vehicle [dimethyl sulfoxide (DMSO)] or with CK-666 (200 μM), inactive CK-689 compound, or CytoD (0.5 μM) or starved in EBSS medium for 60 min. Immunoblots of phosphorylated S6K and 4E-BP1 in MDA-MB-231 (B), BT-549 (C), MCF10A (D), or HT-1080 cells (E) with glyceraldehyde-3-phosphate dehydrogenase (GAPDH) used as a loading control. Plots show the levels of phosphorylated S6K and 4E-BP1 normalized to GAPDH in the different cell lines quantified from at least three independent experiments. (**F**) Distribution of the number of CD63-, Rab7-, VPS35-, and mTOR-positive vesicular structures per cell from images acquired by three dimensional (3D) deconvolution wide-field microscopy. The medians and quartiles are shown in violin plots. All numerical data and statistical tests are provided in table S5.

666 on mTORC1 activity was dose dependent, while CytoD effect was already maximal at the lowest dosage (fig. S2, C and D, quantified in fig. S2, I and J). Inhibition by CK-666 was maximal after 30 min (fig. S2E). LatA treatment, which reduced F-actin/WASH association with endolysosomes, also correlated with a time-dependent reduction of mTORC1 activity (fig. S2, F and G).

These observations were generalized to other cell lines including human breast cancer cell line BT-549 (Fig. 2C), nontransformed MCF10A breast epithelial cells (Fig. 2D), and HT-1080 fibrosarcoma cells (Fig. 2E). A dose-dependent inhibition of mTORC1 activity by CK-666 was observed in all three cell lines, while the lowest dose of CytoD had already the maximal effect, except in MCF10A cells that appeared largely resistant to CytoD in the concentration range

tested (Fig. 2, C to E, and fig. S2, I and J). Immunofluorescence staining of MCF10A cells revealed that the endolysosomal association of F-actin and mTOR was lost upon CK-666 treatment while it persisted in CytoD-treated cells, providing a possible explanation for MCF10A cell resistance to CytoD treatment (fig. S2K). The reversibility of the drug was tested in MDA-MB-231 cells by washing out CK-666 after 60 min; full mTORC1 activity was restored after 15- to 30-min washout of the drug (Fig. 2A and fig. S2H). Collectively, these data demonstrate that acute treatment with drugs that target distinct steps of the branched actin assembly cycle leads to mTORC1 repression in different cellular contexts. All subsequent experiments were performed using 200 μM CK-666 and 0.5 μM CytoD for 60 min.

mTORC1 shuttles between the cytosol and the endolysosomal surface depending on nutrient availability (*38*). Thus, we analyzed the effects of actin drugs on the cellular distribution of mTORC1 signaling components in relation with the endolysosomal compartments. We found no effect of CK-666 and CytoD treatment on the number of Rab7 and VPS35-positive vesicles in MDA-MB-231 cells, while we only saw a modest effect of CK-666 on the number of CD63-positive vesicles, indicating that actin integrity was generally not required for endosomal association of these markers (Fig. 2F). Strikingly, CK-666, CytoD, or LatA treatments strongly impaired mTOR association with endolysosomes, alike starvation (Fig. 2, A and F, and fig. S2F). Furthermore, upon CK-666 washout, endolysosomal F-actin and mTOR-enriched puncta were recovered (Fig. 2A), coinciding with the restoration of mTORC1 activity (fig. S2H). Together, our data support a causal relationship between branched actin puncta and stable association and activity of mTORC1 on endolysosomes in several cell lines.

## mTORC1 signaling requires coincidence with WASH complex on endolysosomes

Given this uncovered role of branched actin in mTORC1 activation, we sought to decipher the contribution of endolysosomal versus lamellipodial actin networks. To alter specifically endolysosomal branched actin, the WASH complex was disrupted by knocking down its WASH subunit, while we targeted the WASP family verprolin homologous (WAVE) regulatory complex responsible for lamellipodial branched actin assembly by KD of two essential subunits, BRK1 and NCKAP1 (Fig. 3A). Silencing of WASH, but not WAVE complex, specifically impaired pS6K and p4E-BP1 levels (Fig. 3A). At the single-cell level, WASH KD correlated with impaired mTOR recruitment on endolysosomes and a reduction of p4E-BP1 level (Fig. 3, B to E). A similar effect was observed upon Arp2/3 complex inactivation through ARPC2 KD, but not upon silencing of lamellipodial actin nucleation-promoting factor, WAVE (Fig. 3, B to E). Collectively, our data demonstrated a specific requirement for WASH-dependent, Arp2/3 branched actin dynamics for mTORC1 association and function on endolysosomes.

We further addressed the regulation of mTORC1 signaling by Arp2/3, WASH complex-dependent endolysosomal F-actin. Early work in human cervical carcinoma Hela cells reported an association of WASH-Arp2/3 complex F-actin networks with the early endosomal recycling pathway (*14*). Along this line, extensive colocalization of WASH complex subunit, FAM21, with early endosome marker EEA1 was observed in HeLa cells (Fig. 3F), in contrast to the limited EEA1/FAM21 overlap in MDA-MB-231 cells (Fig. 3F). Reciprocally, we found little overlap between FAM21 and the endolysosomal marker CD63 in HeLa cells (Fig. 3G). In addition, strong mTOR association with CD63-positive compartments was observed, while mTOR was marginally detected on EEA1-positive early endosomes, indicating that the typical endolysosomal distribution of mTORC1 was retained in HeLa cells (Fig. 3, H and I). Strikingly, while starvation repressed mTORC1 activity and led to mTOR detachment from endolysosomes, lysosomal association and full activity of mTOR were retained in HeLa cells treated with CK-666 or CytoD while the expected actin cytoskeleton disruptions were observed (Fig. 3J and fig. S3A). Together, these data demonstrated that regulation of mTORC1 signaling by endosomal actin requires coincidence of WASH-Arp2/3 complex and mTORC1 signaling components on the endolysosomal membrane system.

## Arp2/3 complex inhibition results in RAGC dissociation from endolysosomal membranes

Endolysosomal association and activation of mTORC1 requires the LAMTOR complex and the association and function of the RAG dimer on the lysosomal surface (*5*, *39*). We addressed the effects of actin drugs on the distribution of LAMTOR4 subunit by immunofluorescence analysis. LAMTOR4 associated with CD63-, F-actin–positive endolysosomes in the perinuclear region in both nutrient replete and depleted cells (Fig. 4, A and B, and fig. S4A). Treatment with CK-666 or CytoD did not affect the LAMTOR4 vesicular signal (Fig. 4, A and B, and fig. S4A). Proximity ligation assay (PLA) was carried out as an independent approach to assess the effect of actin perturbation on LAMTOR4. VPS35 was used as a reference marker as its distribution remained unaffected upon CK-666 treatment (Fig. 2F). In addition, PLA confirmed that proximity between the two Retromer core components: VPS35 and VPS26 resisted actin disruption upon CK-666 treatment (fig. S4, B and C). Robust PLA signal was detected between VPS35 and LAMTOR4 in the vicinity of perinuclear F-actin puncta (fig. S4, D and E). PLA signal was abolished by omission of one of two primary antibodies (fig. S4, E to G) or upon VPS35 or LAMTOR4 KD (fig. S4, F and G), demonstrating the specificity of the PLA reactions. The amount of PLA signal between VPS35 and LAMTOR4 was insensitive to CK-666 or CytoD treatment (fig. S4, D and E). In addition, we analyzed the effect of CK-666 on LAMTOR complex integrity at the biochemical level. GFP-LAMTOR1 or FLAG-LAMTOR4 were transiently expressed in MDA-MB-231 cells, and proteins were immunoprecipitated using the GFP- or FLAG-Trap procedures, respectively, from cells incubated with vehicle [dimethyl sulfoxide (DMSO)] or CK-666 for 60 min before lysis. CK-666 treatment did not affect LAMTOR1/4 interaction (Fig. 4, C and D), nor did it affect $^{GFP}$LAMTOR1 interaction with LAMTOR2 (Fig. 4C). Together, these experiments demonstrate that neither the integrity nor the localization of the LAMTOR complex are affected by branched actin disruption on endolysosomes.

Next, the consequences of actin perturbations on RAGC distribution were analyzed. Contrasting with the situation observed upon nutrient starvation, which tendentially increased RAGC intensity on CD63-positive endolysosomes (Fig. 4, E and F, compare DMSO and EBSS) (*2*, *5*, *6*, *40*), treatment with CK-666 or CytoD significantly impaired vesicular localization of RAGC (Fig. 4, E and F). Last, the capacity of GDP- or GTP-bound RAGC mutants

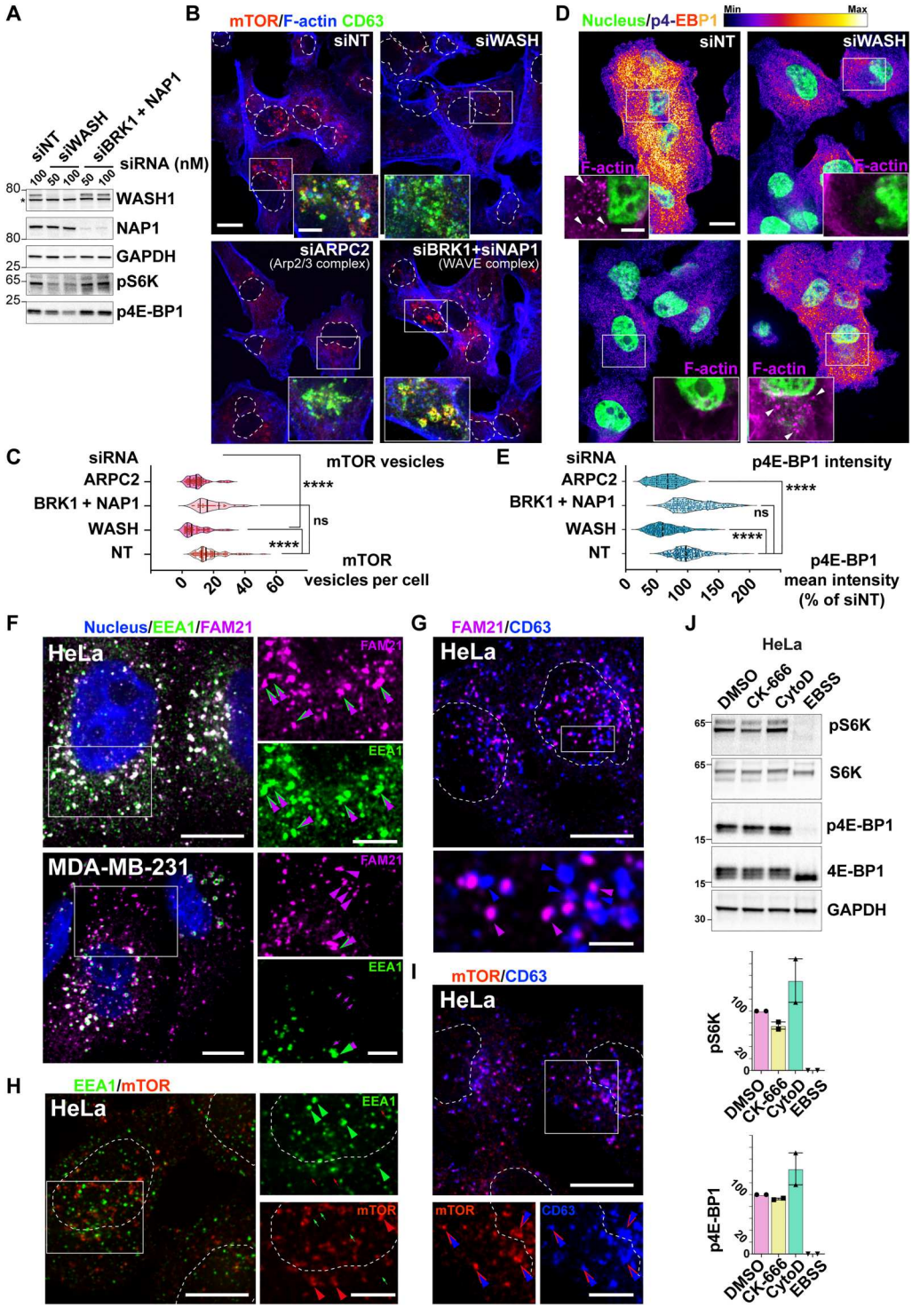


**Fig. 3. Loss of WASH suppresses mTORC1 signaling.** (**A**) MDA-MB-231 cells were treated with control nontargeting siRNA (siNT) or two siRNA concentrations to knock down the WASH subunit of the WASH complex or the BRK1 and NCKAP1 (NAP1) subunits of the WAVE complex. After 72 hours, cells were lysed and analyzed by immunoblotting with the indicated antibodies. GAPDH was used as a loading control. The asterisk points to nonspecific detection. Molecular weight markers are in kDa. (**B**) MDA-MB-231 cells treated with the indicated siRNAs were fixed and stained for F-actin, mTOR, and CD63. (**C**) Quantification of mTOR-positive vesicle/cell from images acquired on a wide-field 3D deconvolution microscope using ImageJ software. (**D**) Cells treated with the indicated siRNAs were fixed and stained for p4E-BP1. Intensity of p4E-BP1 signal is shown using a fire lookup table. (**E**) Quantification of mean intensity of p4E-BP1 immunofluorescence staining in the indicated cell populations. (**F** to **I**) Human cervical cancer HeLa or breast MDA-MB-231 carcinoma cells grown in complete medium were fixed and stained for early endosomal (EEA1) or endolysosomal (CD63) markers and WASH subunit (FAM21) or mTOR kinase as indicated. Scale bars, 10 and 5 μm (insets). (**J**) HeLa cells were treated with vehicle (DMSO) or with CK-666 (200 μM) or CytoD (0.5 μM) or starved in EBSS medium for 60 min. Immunoblots of phosphorylated or total S6K or phosphorylated or total 4E-BP1 with GAPDH used as a loading control. Levels of phosphorylated S6K and 4E-BP1 normalized to GAPDH were quantified from two independent experiments. All numerical data and statistical tests are provided in table S5.

to rescue mTOR endolysosomal distribution and activity was tested. Overexpression of GDP-bound, active, RAGC$^{S75N}$ mutant rescued the inhibitory effect of CK-666 treatment both on p4E-BP1 phosphorylation and vesicular mTOR distribution, in contrast to inactive RAGC$^{Q120L}$ mutant that failed to do so (Fig. 4, G to I, and fig. S5, A and B). Together, our data support an interplay between F-actin puncta and stable association and activity of mTORC1 on endolysosomes and suggest an epistatic relationship between endolysosomal F-actin and the RAGC GTPase.

## DISCUSSION

Our findings bring to light an unprecedented interplay between branched actin dynamics and mTORC1 signaling on

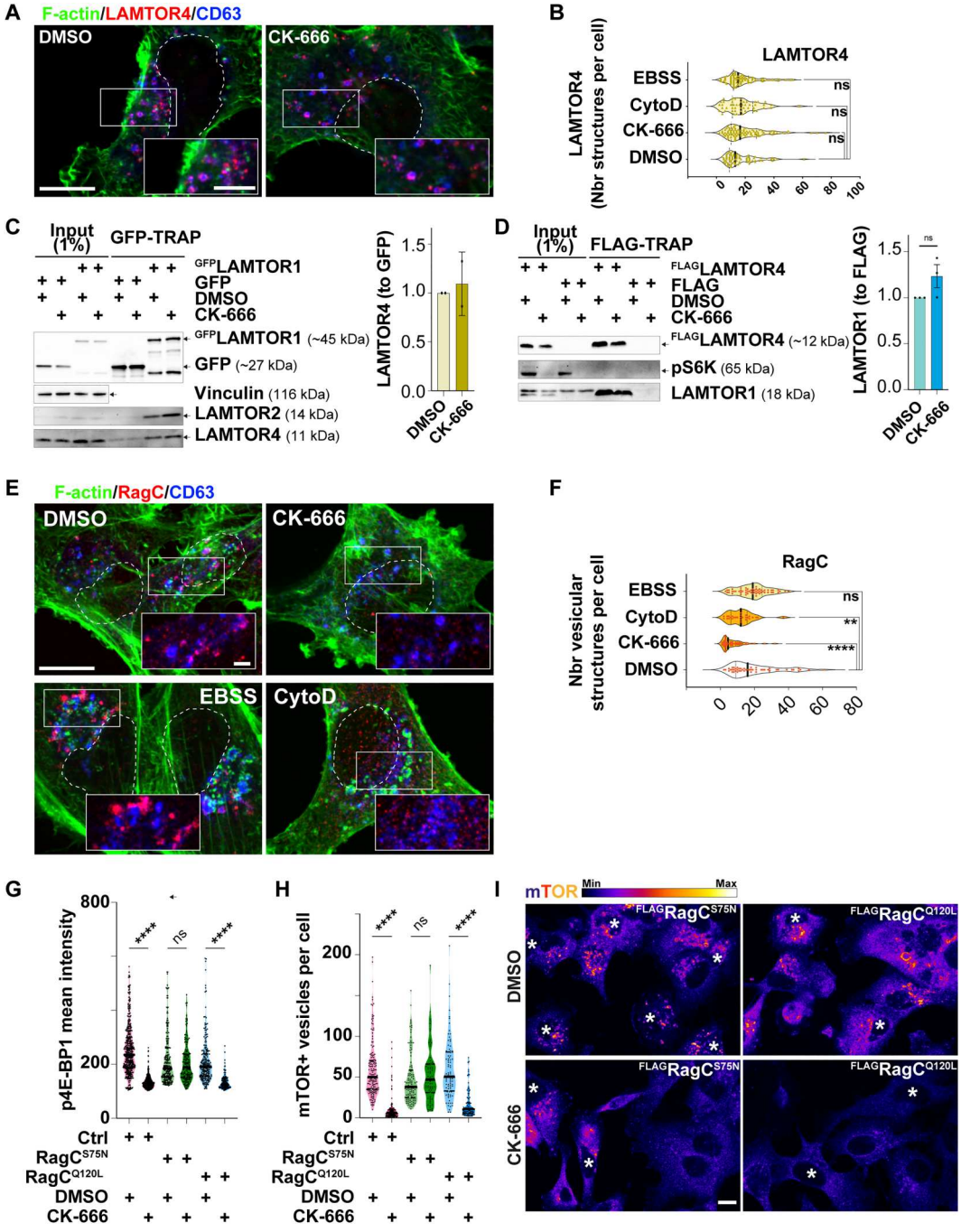


**Fig. 4. RAGC dissociation from endolysosomes upon disruption of the branched actin network.** (**A**) Cells in complete medium were treated with vehicle (DMSO) or with CK-666 for 60 min. After fixation, cells were stained for F-actin, CD63, and LAMTOR4. (**B**) Quantification of LAMTOR4-positive vesicles/cell in cells with the indicated treatment. (**C** and **D**) MDA-MB-231 cells were transfected with vectors expressing GFP-tagged LAMTOR1 (C) or FLAG-tagged LAMTOR4 (D) or corresponding empty vectors. Cells in complete medium were treated with vehicle (DMSO) or CK-666 for 60 min and lysed, and proteins were immunoprecipitated using the GFP- or FLAG-Trap procedure, respectively. Bound partners were detected by immunoblotting with the indicated antibodies. (**E**) MDA-MB-231 cells were stained for F-actin, RAGC, and CD63. The nucleus contour is shown with a dashed line. Scale bars, 10 and 2 μm (insets). (**F**) Quantification of RAGC-positive vesicles/cell in cells with the indicated treatment. (**G** to **I**) MDA-MB-231 cells transiently expressing FLAG-tagged RAGC$^{Q120L}$ or RAGC$^{S75N}$ or transfected with control empty FLAG vector (Ctrl) were fixed and labeled for FLAG tag and p4E-BP1 (see fig. S5, A and B) or mTOR. Quantification of the mean intensity of p4E-BP1 staining in the indicated cell population normalized to the mean intensity in control cells in (G). Number of mTOR-positive vesicular structures per cell in (H). Median and quartiles shown in the violin plots. Intensity of mTOR signal is shown using a fire lookup table in (I). Asterisk denotes FLAG-positive cell. Scale bar, 10 μm (I). All numerical data and statistical tests are provided in table S5.

endolysosomes. Several key mTORC1 signaling components including mTOR kinase and its regulators, RAGC and LAMTOR complex subunits (LAMTOR1 and LAMTOR4), displayed a punctate localization in submicrometric domains in the vicinity of and partially overlapping with WASH/Arp2/3 complex-enriched F-actin puncta on the surface of juxtanuclear endolysosomes. Analysis of the RAGC-associated protein interaction network provided a first hint for an intersection with branched actin dynamics as RAGC interacted and its localization overlapped with actin-capping CAPZA/B proteins on endolysosomes (*31*). A functional regulatory role in barbed end capping was supported by the observation that RAGC silencing led to branched actin puncta enlargement on endolysosomes, reminiscent of actin network elongation observed upon loss of CAPZA/B protein function, although the effect of RAGC KD was milder (*41*–*43*). In addition, loss of perinuclear F-actin puncta upon expression of GDP-bound $RAGC^{S75N}$ (but not GTP-bound $RAGC^{Q120L}$) suggested that active RAGC promoted actin filament capping and prevented filament elongation on endolysosomes, possibly bringing CAPZ CPs and positive regulators, CD2AP and SH3KBP1, together. RAGC, depending on its nucleotide-binding status, may thus influence actin-dependent processes on endolysosomes such as vesicle movement and sorting of endocytic receptors in the recycling pathway (*25*, *26*, *41*–*46*). Moreover, branched actin networks can deform the underlying lipid bilayer; a property that is in line with the role of retromer and WASH complexes in the fission of endocytic recycling transport intermediates (*15*, *24*, *47*, *48*). Together, our data suggest potential previously unidentified functions for RAGC in endocytic recycling of membrane receptors that will deserve further investigation.

In a broader perspective, actin filaments also fulfill an organizational role at membranes by immobilization of specific proteins into signaling networks, which can cluster into distinct subdomains and influence signaling outputs including in the context of mTORC1 regulation of proteostasis (*49*–*52*). With this in mind, we investigated and established a modulation of mTORC1 localization and function by endolysosomal F-actin. Widely used inhibitors targeting different steps of the branched actin polymerization reaction, namely, Arp2/3 complex-dependent actin nucleation (CK-666), filament assembly (LatA), and barbed end capping (CytoD), dissociated mTOR from endolysosomes and acutely repressed mTORC1 activity. Moreover, the fact that the effect of actin drugs was fully reversible (upon washout) and that KD of the WASH complex, but not the WAVE complex, phenocopied the drugs indicates that mTORC1 dependency on actin is direct and restricted to the endolysosomal branched actin network.

On a mechanistic standpoint, in contrast to low-nutrient conditions, in which RAGC remains stably anchored to the endolysosomal surface [Fig. 4, E and F and (*2*, *5*, *6*, *40*)], perturbation of endolysosomal actin dynamics under nutrient replete conditions did not affect LAMTOR distribution but led to the detachment of RAGC from endolysosomes in line with mTORC1 inhibition. Similarly, lysosome dissociation of RAGC and mTOR has been previously reported in retromer-deficient cells (*30*). A mechanism was proposed that implicated the regulation of Rab7 localization and activity by retromer that could impinge on mTORC1 function (*30*). We believe that these observations could also be interpreted in light of the key role of retromer in WASH complex recruitment and F-actin assembly on endolysosomes and based on our data linking mTORC1 function to the integrity of the endolysosomal actin network (*13*, *20*, *21*).

The fact that overexpression of active, GDP-bound $RAGC^{S75N}$ rescued mTORC1 activity emphasized a complex reciprocal interplay whereby active RAGC controls branched actin assembly through regulation of filament capping, while the presence of branched actin is necessary for RAGC association to the endolysosome surface. How perturbation of actin dynamics could lead to RAGC dissociation from endolysosomal membranes is not currently understood. SLC38A9 and v-ATPase work together to regulate the activity of Rag GTPases on endolysosomes (*6*, *7*). In addition, v-ATPase interacts with both actin and WASH through its $V_1$ domain (*18*, *44*, *53*), suggesting a potential role for v-ATPase in the dependency of RAGC association to endolysosomes on F-actin. Moreover, whether regulation of actin filament capping by RAGC could contribute to the control of mTORC1 activity remains an open question as RAGC silencing, which affects actin capping, also primarily interferes with the tethering of mTORC1 on endolysosomes. We also report that mTORC1 regulation by endolysosomal branched actin was intriguingly inoperant in HeLa cells. A distinctive feature of HeLa cells is the preferential association of the WASH-Arp2/3 complex module to the early endocytic pathway in relation with a role in early endocytic recycling of membrane receptors (*14*). This is in contrast to a mostly endolysosomal distribution of WASH-Arp2/3 in several cell lines that we examined and also reported in different cell types in various animal species (*18*, *44*, *54*–*56*). Consequently, there was minimal coincidence between the WASH-Arp2/3 and mTORC1 modules in HeLa cells, while they strongly overlapped in other cell types underlying the principle of actin-based regulation of mTORC1 in these cells.

## MATERIALS AND METHODS

### Reagents and antibodies

The source and conditions of utilization of reagents used in this study are listed in table S2. Antibodies are listed in table S3.

### Cell culture

Cell lines were obtained from the American Type Culture Collection (ATCC). The absence of mycoplasma contamination was routinely verified by polymerase chain reaction. Triple-negative human breast cancer MDA-MB-231 cells (ATCC HTB-26) were cultured in Leibovitz L-15 medium with 15% fetal bovine serum (FBS) and 2 mM glutamine at 37°C with 1% $CO_2$. HT-1080 fibrosarcoma cells (ATCC CCL-121) and human embryonic kidney 293 T/17 cells (ATCC CRL-11268) were cultured in Dulbecco's modified Eagle's medium (DMEM) with GlutaMAX supplement with 10% FBS and 2 mM glutamine at 37°C with 5% $CO_2$. The triple-negative human breast ductal carcinoma cell line, BT-549 (ATCC HTB-122), was cultured with RPMI 1640 medium containing 10% FBS, 1 mM sodium pyruvate, and 2 mM glutamine at 37°C with 5% $CO_2$. Human MCF10A epithelial breast cells (ATCC CRL-10317) were maintained in DMEM-F12 containing 1× penicillin/streptomycin, 2 mM glutamine, human insulin (10 μg/ml), cholera toxin (100 ng/ml), hydrocortisone (0.5 μg/ml), 5% horse serum, and epidermal growth factor (20 ng/ml) at 37°C with 1% $CO_2$. For starvation, cells were washed two times with phosphate-buffered saline (PBS) followed by incubation in EBSS for 1 hour at 37°C.

### Transfection and siRNA treatment

For transient expression, MDA-MB-231 cells were transfected with plasmid DNA using Lipofectamine 3000 according to the manufacturer's instructions. Briefly, cells were trypsinized and $1.5 \times 10^5$ cells were plated in a 24-well plate. The transfection mixture containing Lipofectamine 3000 together with P3000 reagent and 0.5 μg of DNA was incubated for 10 min and added to 24-well plate together with the cell suspension. The transfection mixture was replaced with culture medium 15 hours later. Cells were analyzed 36 to 48 hours after transfection. Mouse CD2AP N-terminally tagged with enhanced green fluorescent protein (EGFP) cloned in pEGFP-C1 vector was a gift of M. Cormont (INSERM, Nice). P-eGFP-beta 2 CP encoding mouse Capzb with an N-terminal EGFP tag was a gift from J. Cooper (Addgene plasmid #13298). Plasmid FLAG-HA-pcDNA3.1- was a gift from A. Antebi (Addgene plasmid #52535), plasmids pRK5 Flag-RAGC(S75N) (Addgene plasmid #99724), pRK5 Flag RAGC(Q120L) (Addgene plasmid #99725), N1-p18-EGFP (Addgene plasmid #42334, GFP-LAMTOR1), and pRK5-FLAG-C7orf59 (Addgene plasmid #42332, FLAG-LAMTOR4) were provided by D. Sabatini (*7*, *57*).

For silencing experiments, cells were treated with the indicated small interfering RNA (siRNA) or SMARTpool mix (50 to 100 nM, listed in table S4) using Lullaby reagent according to the manufacturer's instructions. The siRNA/lullaby mix was incubated for 30 min and added to the well followed by the addition of the cell suspension ($4 \times 10^4$ cells were plated in 24-well plate or $8 \times 10^4$ cells in 12-well plate). Cells were analyzed after 72 hours of treatment.

### Drug treatment

One day before the experiment, cells were plated on 12-mm-diameter glass coverslip in a 24-well plate ($6 \times 10^4$ cells per well in 0.5 ml of complete medium) or an 18-mm-diameter glass coverslip in a 12-well plate ($9 \times 10^4$ cells per well in 1 ml of medium). Then, the fresh medium was added to the well, and cells were treated with the vehicle or with the different actin drugs for 1 hour in complete medium at 37°C (see table S2). If not indicated otherwise, working concentration was 200 μM CK-666 and 0.5 μM CytoD. For washout experiments, cells were treated with CK-666 for 1 hour, washed several times in complete medium without the drug, and incubated for 15 min to 2 hours after washout. Cells were processed for immunoblotting or immunofluorescence analysis as described below.

### Indirect immunofluorescence analysis and imaging of fixed samples

Cells were plated on 12-mm-diameter glass coverslips in 24-well plate ($6 \times 10^4$ cells per well) or on 18-mm-diameter glass coverslips in 12-well plate ($1.2 \times 10^5$ cells per well), 1 day before the experiment. After the indicated treatment, cells were washed once with PBS and fixed with 4% paraformaldehyde in PBS for 15 min at room temperature (RT). Cells were washed with PBS three times and then permeabilized with 0.1% Triton X-100 in PBS for 15 min at RT, followed by washing with PBS. Blocking was done with 15% FBS in PBS or 1% bovine serum albumin in PBS for RAGC, LAMTOR1, and LAMTOR4 antibodies for 1 hour at RT. For anti–p4E-BP1 staining, after fixation in 4% paraformaldehyde, cells were permeabilized with 0.05% saponin (Sigma-Aldrich) in PBS for 10 min. Samples were blocked with 0.05% saponin and 5% fetal calf serum in PBS for 30 min at RT and stained with anti–p4E-BP1 antibodies for 2 hours at RT. Cells were then washed with PBS and incubated with diluted primary antibodies in PBS for 1 hour at RT. The coverslips were washed three times with PBS, followed by incubation with fluorescently labeled conjugated secondary antibodies for 1 hour at RT protected from light. Coverslips were washed three times with PBS and mounted on glass slides with Prolong-DAPI (4′,6-diamidino-2-phenylindole) mounting medium. Images were acquired using a 100× Plan Apo VC 1.4 oil objective with a wide-field microscope (Nikon Eclipse 90i upright) using a cooled interlined charge-coupled device camera (CoolSNAP HQ2, Roper Scientific) or with an inverted Eclipse Ti-E (Nikon) spinning disk confocal microscope (Yokogawa CSU-X1 confocal scanner unit interfaced with Metamorph software, Molecular Devices by Gataca Systems, Massy, France). A z stack of images was taken every 0.2 μm by mean of a piezoelectric motor (Physik Instrumente).

For Airyscan high-resolution imaging, MDA-MB-231 cells were fixed and immunostained as described above. Images were acquired using Zeiss LSM 900 confocal microscope equipped with Airyscan detectors using an oil immersion 63× Plan Apochromat, numerical aperture 1.4 objective. Z stacks were acquired with optimal Airyscan settings for each individual channel. After acquisition, stacks were processed by three dimensional Airyscan processing features in Zeiss Zen software.

### Image analysis

The quantification of vesicles was done using a homemade ImageJ macro. The macro was designed to choose the best planes or *z* projection for specific channels for vesicle detection. The cell contour for each cell in the field was drawn and added to the region of interest Manager. For each individual cell, "fit ellipse" was computed using major horizontal and minor vertical axis and the image was centered on the cell centroid where the two major axes meet. Automatic detection of the vesicles was done on the *z* projection of the transformed image on the chosen channels. *z* planes were projected using maximal intensity projection, and the signal for vesicles was determined using thresholding command excluding regions <50 pixel to avoid nonvesicular background signal. All computation was done for each individual vesicle including "area" and "area mean intensity" using ImageJ commands. For cell center–to–periphery distribution analysis, the line joining the cell centroid (0) and vesicle center was prolonged to the cell contour (1) and the vesicle position was computed on the 0-to-1 axis. The macro is available (https://github.com/Anne-SophieMACE/EndosomalProteinDetection). The mean intensity of p4E-BP1 per cell was quantified using a homemade ImageJ macro. Briefly, cells were manually delimited using the phalloidin signal and the p4E-BP1 mean intensity per cell was measured using the "Measure" command of ImageJ.

### Live cell imaging

MDA-MB-231 cells were treated with siRNAs in 12-well culture dishes as described in the above section. After 42 hours, cells were trypsinized and transiently transfected with indicated plasmids using Lipofectamine 3000. Cells were plated on glass bottom dishes (MatTek Corporation) and imaged after 36 hours. On the day of the experiment, cells were replenished with complete medium

and z stacks of images were acquired every 2 s for 5 min by confocal spinning disk microscopy as described above.

### In situ PLA

MDA-MB-231 cells were plated on 12-mm glass coverslips in 24-well plate 1 day before the assay and then treated with 50 nM siRNA for 72 hours or with actin drugs for 1 hour as described above. After fixation and permeabilization, cells were incubated with a combination of mouse and rabbit primary antibodies targeting the proteins of interest for 1 hour at RT. After three washes with PBS, secondary antibodies tagged with short DNA oligonucleotides (mouse PLUS PLA and rabbit MINUS PLA probes) were incubated in preheated humidity chamber for 1 hour at 37°C. After two 5-min washes with PLA buffer A [150 mM NaCl, 10 mM tris base, and 0.05% Tween 20 (pH 7.4)], ligation was performed for 30 min at 37°C with PLA in situ detection reagent Orange kit. Coverslips were washed twice for 5 min with PLA buffer A. Last, amplification was obtained using polymerase for 100 min at 37°C to generate the PLA signal. Coverslips were washed twice for 10 min with PLA buffer B [100 mM NaCl, 35 mM tris base, and 165 mM tris-HCl (pH 7.4)] and stained with phalloidin–Alexa Fluor 488 for 30 min at RT before mounting in Prolong-DAPI medium. Samples were analyzed on an inverted wide-field microscope as previously described. For quantification of PLA signal, the ImageJ software was used. Briefly, fluorescent PLA signal was thresholded manually and the number of PLA dots was obtained using the Analyze Particles Plugin of ImageJ. The number of dots was then divided by the number of nuclei present in the corresponding acquisition field, and results were normalized to control condition.

### Immunoprecipitation analysis

For endogenous immunoprecipitation analysis, $2 \times 10^6$ MDA-MB-231 cells were plated in a 10-cm-diameter dish 1 day before the experiment. Eight to 10 10-cm dishes were prepared for each condition. On the day of the experiment, dishes were replenished with fresh complete medium and actin drugs were added as above. After 1 hour, cells were washed once with ice-cold PBS on ice and immediately lysed with ice-cold CHAPS lysis buffer [0.3% CHAPS, 10 mM β-glycerol phosphate, 10 mM pyrophosphate, 40 mM Hepes (pH 7.4), 2.5 mM $MgCl_2$, 1 tablet of EDTA-free protease inhibitor per 25 ml and Phosphatase Inhibitor Cocktail 2]. All lysates for a given condition were pooled (~400 μl of cell lysate). Lysates were centrifuged at 130,000 rpm for 10 min at 4°C to remove insoluble and particulate materials. Protein concentration was measured with the bicinchronic acid (BCA) protein assay kit as described before. Primary antibodies [control immunoglobulin G (IgG) or anti-RAGC IgGs] were added to the lysates and incubated with rotation overnight at 4°C. The next day, beads were sedimented by low-speed centrifugation and kept on ice. A total of 60 μl of a 50% slurry of protein G agarose beads (Thermo Fisher Scientific) was washed and equilibrated in lysis buffer. Cell lysates were added to protein G agarose beads in separate 1.5-ml Eppendorf tubes and incubated for 4 hours at 4°C. Then, samples were centrifuged at 2500 rpm for 2 min at 4°C. Immunoprecipitates were washed three times with lysis buffer containing 150 mM NaCl (5 min each followed by centrifugation at 2500 rpm for 5 min at 4°C). Immunoprecipitated proteins were analyzed by MS or denatured in 20 to 30 μl of Laemmli sample–reducing buffer and boiled for 5 min at 95°C, resolved by 4 to 12% SDS–polyacrylamide gel electrophoresis (SDS-PAGE), and analyzed by immunoblotting.

### MS and proteomic analysis

After washes with CHAPS lysis buffer, beads were washed twice with 100 μl of 25 mM $NH_4HCO_3$. Last, beads were resuspended in 100 μl of 25 mM $NH4HCO_3$ and digested with 0.2 μg of trypsine/LysC (Promega) for 1 hour at 37°C. Samples were then loaded into custom-made C18 StageTips packed by stacking one AttractSPE disk (Affinisep) and 2 mg of beads (Cartridge Waters) into a 200-μl micropipette tip for desalting. Peptides were eluted using a ratio of 40:60 MeCN:$H_2O$ + 0.1% formic acid and vacuum-concentrated to dryness. Peptides were reconstituted in injection buffer (2:98 MeCN:$H_2O$ + 0.3% trifluoroacetic acid) before liquid chromatography tandem MS (LC-MS/MS) analysis.

### LC-MS/MS analysis

Online chromatography was performed using the UltiMate 3000 RSLCnano System coupled to an Orbitrap Fusion Tribrid mass spectrometer (Thermo Fisher Scientific). Peptides were trapped in a C18 column (75-μm inner diameter by 2 cm; nanoViper Acclaim PepMap 100, Thermo Fisher Scientific) with buffer A (2:98 MeCN:$H_2O$ in 0.1% formic acid) at a flow rate of 3.0 μl/min over 4 min. Separation was performed using a 40 cm by 75 μm C18 column (Reprosil C18, 1.9 μm, 120 Å, Pepsep PN: PSC-40-75-1.9-UHP-nC), regulated to a temperature of 40°C with a linear gradient of 3 to 32% buffer B (100% MeCN in 0.1% formic acid) at a flow rate of 150 nl /min over 91 min. Full-scan MS was acquired using an Orbitrap analyzer with the resolution set to 120,000. Ions from each full scan were fragmented with higher-energy C-trap dissociation and analyzed in the linear ion trap.

For identification, data were searched against the *Homo sapiens* UP000005640 database using Sequest HT through Proteome Discoverer (v.2.4). The enzyme specificity was set to trypsin, and a maximum of two missed cleavage sites were allowed. Oxidized methionine, N-terminal acetylation, methionine loss, and methionine acetylation loss were set as variable modifications. Maximum allowed mass deviation was set to 10 parts per million for monoisotopic precursor ions and 0.6 Da for MS/MS peaks. The resulting files were further processed using myProMS v.3.9.2 (https://github.com/bioinfo-pf-curie/myproms) (*58*). False discovery rate (FDR) was calculated using a percolator (*59*) and was set to 1% at peptide level for the whole study. Label-free quantification was performed using peptide extracted ion chromatograms (XICs) computed with MassChroQ v.2.2.21 (*60*). For protein quantification, XICs from proteotypic peptides shared between compared conditions (TopN matching) with missed cleavages were used. Median and scale normalization at peptide level were applied on the total signal to correct the XICs for each biological replicate ($N = 3$). To estimate the significance of the change in protein abundance, a linear model (adjusted on peptides and biological replicates) was performed and $P$ values were adjusted using the Benjamini-Hochberg FDR procedure. Proteins with at least three total peptides in all three independent replicates, a 1.6-fold enrichment, and an adjusted $P$ value $\leq 0.05$ were considered significantly enriched in sample comparisons. Unique proteins were considered with at least three total peptides in all three replicates. Protein selected with these criteria were further analyzed with Cytoscape (version 3.8.2). The MS

proteomics raw data have been deposited to the ProteomeXchange Consortium via the PRIDE partner repository with the dataset identifier PXD027100 (reviewer_pxd027100@ebi.ac.uk, password: cami1Wqx) (*61*).

### Cell lysis and immunoblotting

At the end of the treatment or 72 hours after silencing, cells were placed on ice, washed with ice-cold PBS, and gently scraped using radioimmunoprecipitation assay (RIPA) buffer [50 mM tris-HCl (pH 8.0), 137 mM NaCl, 1% Triton, 10 mM $MgCl_2$, 10% glycerol, Protease Inhibitor Cocktail tablet, and Phosphatase Inhibitor Cocktail 2 added freshly). Cells were incubated on a spinning rotator for 30 min at 4°C for lysis, followed by centrifugation at 140,000 rpm at 4°C. The supernatant was collected in a fresh tube. Protein concentration was measured using Pierce BCA protein assay kit. Laemmli sample–reducing buffer was added, and samples were heated for 5 min at 95°C and analyzed by SDS-PAGE. Proteins in the lysate (1 μg) were separated using NUPAGE 4 to 12% tris-glycine gels and transferred on a nitrocellulose membrane using the iBlot2 Dry Blotting System. The membrane was incubated for 2 hours in blocking buffer [5% (w/v) BSA in tris buffer saline (pH 7.4) and 1% Tween 20 (TBST)], followed by primary antibody incubation at RT or overnight incubation at 4°C in TBST. Then, the membrane was washed and incubated with horseradish peroxidase–conjugated secondary antibodies diluted in blocking buffer for 1 hour at RT. After three washes with TBST, antibodies were detected using the enhanced chemiluminescence reagent using the ChemiDoc MP Imaging System (Bio-Rad).

### FLAG- and GFP-Trap procedures

MDA-MB-231 cells transfected with FLAG-tag vectors were lysed in 300 μl of 1% NP-40 lysis buffer [50 mM tris-HCl (pH 7.5), 150 mM NaCl, 0.5 mM EDTA, 10 mM $MgCl_2$, 10% glycerol, 1% NP-40, EDTA-free protease inhibitor tablet, and Phosphatase Inhibition Cocktail 2]. Lysates were centrifuged at 13,000 rpm for 10 min at 4°C, and 50 μl of the supernatant was kept as input. The lysate was incubated with 25 μl of equilibrated binding control agarose beads (ChromoTek #bab-20) for 30 min at 4°C under constant agitation. The precleared lysate was then incubated with 25 μl of equilibrated anti-FLAG tag Fab-Trap agarose beads (ChromoTek) for 1 hour at 4°C. Fab-Trap beads were washed twice with 0.7% NP-40 washing buffer, followed by two washes with the same buffer without NP-40. The procedure for GFP-Trap assay was identical except that NP-40 lysis buffer was replaced by 0.3% CHAPS lysis buffer [0.3% CHAPS, 10 mM β-glycerol phosphate, 10 mM pyrophosphate, 40 mM Hepes (pH 7.4), 2.5 mM $MgCl_2$, 1 tablet of EDTA-free protease inhibitor per 25 ml, and Phosphatase Inhibitor Cocktail 2]. Precleared lysate was incubated with 25 μl of equilibrated anti-GFP nanobody agarose beads coupled to (GFP-Trap, ChromoTek) for 1 hour at 4°C. Beads were washed twice with 0.15% CHAPS-containing buffer followed by two washes without detergent. Proteins bound to the beads were boiled at 95°C for 10 min in Laemmli sample–reducing buffer and used for immunoblotting analysis.

### Statistics and reproducibility

All data are presented as means ± SEM from at least three independent experiments except indicated otherwise. GraphPad Prism software was used for statistical analysis. Data were tested for normal distribution using the parametric and nonparametric tests. One-way analysis of variance (ANOVA), Kruskal-Wallis, or Mann-Whitney tests were applied as summarized in table S5. Statistical significance was defined as $*P < 0.05$, $**P < 0.01$, $***P < 0.001$, and $****P < 0.0001$; ns, nonsignificant.

## Supplementary Materials

**This PDF file includes:**

Figs. S1 to S5
Legends for tables S1 and S5
Tables S2 to S4
Legend for movie S1
Macro for vesicle quantification

**Other Supplementary Material for this manuscript includes the following:**

Tables S1 and S5
Movie S1

## REFERENCES AND NOTES


1. G. Y. Liu, D. M. Sabatini, mTOR at the nexus of nutrition, growth, ageing and disease. *Nat. Rev. Mol. Cell Biol.* **21**, 183–203 (2020).
2. O. A. Brady, H. I. Diab, R. Puertollano, Rags to riches: Amino acid sensing by the Rag GTPases in health and disease. *Small GTPases* **7**, 197–206 (2016).
3. S. A. Fernandes, C. Demetriades, The Multifaceted Role of Nutrient Sensing and mTORC1 Signaling in Physiology and Aging. *Front. Aging* **2**, 707372 (2021).
4. P. Gollwitzer, N. Grutzmacher, S. Wilhelm, D. Kummel, C. Demetriades, A Rag GTPase dimer code defines the regulation of mTORC1 by amino acids. *Nat. Cell Biol.* **24**, 1394–1406 (2022).
5. Y. Sancak, L. Bar-Peled, R. Zoncu, A. L. Markhard, S. Nada, D. M. Sabatini, Ragulator-Rag complex targets mTORC1 to the lysosomal surface and is necessary for its activation by amino acids. *Cell* **141**, 290–303 (2010).
6. R. Zoncu, L. Bar-Peled, A. Efeyan, S. Wang, Y. Sancak, D. M. Sabatini, mTORC1 senses lysosomal amino acids through an inside-out mechanism that requires the vacuolar H(+)-ATPase. *Science* **334**, 678–683 (2011).
7. L. Bar-Peled, L. D. Schweitzer, R. Zoncu, D. M. Sabatini, Ragulator is a GEF for the rag GTPases that signal amino acid levels to mTORC1. *Cell* **150**, 1196–1208 (2012).
8. Y. Xu, A. Parmar, E. Roux, A. Balbis, V. Dumas, S. Chevalier, B. I. Posner, Epidermal growth factor-induced vacuolar (H+)-atpase assembly: A role in signaling via mTORC1 activation. *J. Biol. Chem.* **287**, 26409–26422 (2012).
9. S. Wang, Z. Y. Tsun, R. L. Wolfson, K. Shen, G. A. Wyant, M. E. Plovanich, E. D. Yuan, T. D. Jones, L. Chantranupong, W. Comb, T. Wang, L. Bar-Peled, R. Zoncu, C. Straub, C. Kim, J. Park, B. L. Sabatini, D. M. Sabatini, Metabolism. Lysosomal amino acid transporter SLC38A9 signals arginine sufficiency to mTORC1. *Science* **347**, 188–194 (2015).
10. K. Shen, D. M. Sabatini, Ragulator and SLC38A9 activate the Rag GTPases through noncanonical GEF mechanisms. *Proc. Natl. Acad. Sci. U.S.A.* **115**, 9545–9550 (2018).
11. Z. Y. Tsun, L. Bar-Peled, L. Chantranupong, R. Zoncu, T. Wang, C. Kim, E. Spooner, D. M. Sabatini, The folliculin tumor suppressor is a GAP for the RagC/D GTPases that signal amino acid levels to mTORC1. *Mol. Cell* **52**, 495–505 (2013).
12. C. Demetriades, N. Doumpas, A. A. Teleman, Regulation of TORC1 in response to amino acid starvation via lysosomal recruitment of TSC2. *Cell* **156**, 786–799 (2014).
13. T. S. Gomez, D. D. Billadeau, A FAM21-Containing WASH Complex Regulates Retromer-Dependent Sorting. *Dev. Cell* **17**, 699–711 (2009).
14. E. Derivery, C. Sousa, J. J. Gautier, B. Lombard, D. Loew, A. Gautreau, The Arp2/3 Activator WASH Controls the Fission of Endosomes through a Large Multiprotein Complex. *Dev. Cell* **17**, 712–723 (2009).
15. E. Derivery, E. Helfer, V. Henriot, A. Gautreau, Actin Polymerization Controls the Organization of WASH Domains at the Surface of Endosomes. *PLOS ONE* **7**, e39774 (2012).
16. T. S. Gomez, J. A. Gorman, A. A. de Narvajas, A. O. Koenig, D. D. Billadeau, Trafficking defects in WASH-knockout fibroblasts originate from collapsed endosomal and lysosomal networks. *Mol. Biol. Cell* **23**, 3215–3228 (2012).
17. M. Hernandez-Valladares, T. Kim, B. Kannan, A. Tung, A. H. Aguda, M. Larsson, J. A. Cooper, R. C. Robinson, Structural characterization of a capping protein interaction motif defines a family of actin filament regulators. *Nat. Struct. Mol. Biol.* **17**, 497–503 (2010).

18. L. Park, P. A. Thomason, T. Zech, J. S. King, D. M. Veltman, M. Carnell, S. Ura, L. M. Machesky, R. H. Insall, Cyclical Action of the WASH Complex: FAM21 and Capping Protein Drive WASH Recycling, Not Initial Recruitment. *Dev. Cell* **24**, 169–181 (2013).
19. A. I. Fokin, V. David, K. Oguievetskaia, E. Derivery, C. E. Stone, L. Cao, N. Rocques, N. Molinie, V. Henriot, M. Aumont-Nicaise, M. V. Hinckelmann, F. Saudou, C. Le Clainche, A. P. Carter, G. Romet-Lemonne, A. M. Gautreau, The Arp1/11 minifilament of dynactin primes the endosomal Arp2/3 complex. *Sci. Adv.* **7**, eabd5956 (2021).
20. M. E. Harbour, S. Y. Breusegem, M. N. Seaman, Recruitment of the endosomal WASH complex is mediated by the extended 'tail' of Fam21 binding to the retromer protein Vps35. *Biochem. J.* **442**, 209–220 (2012).
21. E. Helfer, M. E. Harbour, V. Henriot, G. Lakisic, C. Sousa-Blin, L. Volceanov, M. N. J. Seaman, A. Gautreau, Endosomal recruitment of the WASH complex: Active sequences and mutations impairing interaction with the retromer. *Biol. Cell* **105**, 191–207 (2013).
22. F. Steinberg, M. Gallon, M. Winfield, E. C. Thomas, A. J. Bell, K. J. Heesom, J. M. Tavare, P. J. Cullen, A global analysis of SNX27-retromer assembly and cargo specificity reveals a function in glucose and metal ion transport. *Nat. Cell Biol.* **15**, 461–471 (2013).
23. M. N. Seaman, The retromer complex - endosomal protein recycling and beyond. *J. Cell Sci.* **125**(Pt 20), 4693–4702 (2012).
24. P. J. Cullen, F. Steinberg, To degrade or not to degrade: Mechanisms and significance of endocytic recycling. *Nat. Rev. Mol. Cell Biol.* **19**, 679–696 (2018).
25. M. A. Puthenveedu, B. Lauffer, P. Temkin, R. Vistein, P. Carlton, K. Thorn, J. Taunton, O. D. Weiner, R. G. Parton, M. von Zastrow, Sequence-Dependent Sorting of Recycling Proteins by Actin-Stabilized Endosomal Microdomains. *Cell* **143**, 761–773 (2010).
26. T. Zech, S. D. Calaminus, P. Caswell, H. J. Spence, M. Carnell, R. H. Insall, J. Norman, L. M. Machesky, The Arp2/3 activator WASH regulates α5β1-integrin-mediated invasive migration. *J. Cell Sci.* **124**(Pt 22), 3753–3759 (2011).
27. P. Monteiro, C. Rosse, A. Castro-Castro, M. Irondelle, E. Lagoutte, P. Paul-Gilloteaux, C. Desnos, E. Formstecher, F. Darchen, D. Perrais, A. Gautreau, M. Hertzog, P. Chavrier, Endosomal WASH and exocyst complexes control exocytosis of MT1-MMP at invadopodia. *J. Cell Biol.* **203**, 1063–1079 (2013).
28. M. N. Seaman, M. E. Harbour, D. Tattersall, E. Read, N. Bright, Membrane recruitment of the cargo-selective retromer subcomplex is catalysed by the small GTPase Rab7 and inhibited by the Rab-GAP TBC1D5. *J. Cell Sci.* **122**(Pt 14), 2371–2382 (2009).
29. A. Jimenez-Orgaz, A. Kvainickas, H. Nagele, J. Denner, S. Eimer, J. Dengjel, F. Steinberg, Control of RAB7 activity and localization through the retromer-TBC1D5 complex enables RAB7-dependent mitophagy. *EMBO J.* **37**, 235–254 (2018).
30. A. Kvainickas, H. Nagele, W. Qi, L. Dokladal, A. Jimenez-Orgaz, L. Stehl, D. Gangurde, Q. Zhao, Z. Hu, J. Dengjel, C. De Virgilio, R. Baumeister, F. Steinberg, Retromer and TBC1D5 maintain late endosomal RAB7 domains to enable amino acid-induced mTORC1 signaling. *J. Cell Biol.* **218**, 3019–3038 (2019).
31. M. Edwards, A. Zwolak, D. A. Schafer, D. Sept, R. Dominguez, J. A. Cooper, Capping protein regulators fine-tune actin assembly dynamics. *Nat. Rev. Mol. Cell Biol.* **15**, 677–689 (2014).
32. Y. Sancak, T. R. Peterson, Y. D. Shaul, R. A. Lindquist, C. C. Thoreen, L. Bar-Peled, D. M. Sabatini, The Rag GTPases bind raptor and mediate amino acid signaling to mTORC1. *Science* **320**, 1496–1501 (2008).
33. B. J. Nolen, N. Tomasevic, A. Russell, D. W. Pierce, Z. Jia, C. D. McCormick, J. Hartman, R. Sakowicz, T. D. Pollard, Characterization of two classes of small molecule inhibitors of Arp2/3 complex. *Nature* **460**, 1031–1034 (2009).
34. M. F. Carlier, P. Criquet, D. Pantaloni, E. D. Korn, Interaction of cytochalasin D with actin filaments in the presence of ADP and ATP. *J. Biol. Chem.* **261**, 2041–2050 (1986).
35. M. Coue, S. L. Brenner, I. Spector, E. D. Korn, Inhibition of actin polymerization by latrunculin A. *FEBS Lett.* **213**, 316–318 (1987).
36. C. T. Wu, H. Y. Chen, T. K. Tang, Myosin-Va is required for preciliary vesicle transportation to the mother centriole during ciliogenesis. *Nat. Cell Biol.* **20**, 175–185 (2018).
37. C. Colombero, D. Remy, S. Antoine-Bally, A. S. Mace, P. Monteiro, N. ElKhatib, M. Fournier, A. Dahmani, E. Montaudon, G. Montagnac, E. Marangoni, P. Chavrier, mTOR Repression in Response to Amino Acid Starvation Promotes ECM Degradation Through MT1-MMP Endocytosis Arrest. *Adv. Sci.* **8**, e2101614 (2021).
38. B. Carroll, Spatial regulation of mTORC1 signalling: Beyond the Rag GTPases. *Semin. Cell Dev. Biol.* **107**, 103–111 (2020).
39. M. E. G. de Araujo, A. Naschberger, B. G. Furnrohr, T. Stasyk, T. Dunzendorfer-Matt, S. Lechner, S. Welti, L. Kremser, G. Shivalingaiah, M. Offterdinger, H. H. Lindner, L. A. Huber, K. Scheffzek, Crystal structure of the human lysosomal mTORC1 scaffold complex and its impact on signaling. *Science* **358**, 377–381 (2017).
40. R. E. Lawrence, K. F. Cho, R. Rappold, A. Thrun, M. Tofaute, D. J. Kim, O. Moldavski, J. H. Hurley, R. Zoncu, A nutrient-induced affinity switch controls mTORC1 activation by its Rag GTPase-Ragulator lysosomal scaffold. *Nat. Cell Biol.* **20**, 1052–1063 (2018).
41. J. Taunton, B. A. Rowning, M. L. Coughlin, M. Wu, R. T. Moon, T. J. Mitchison, C. A. Larabell, Actin-Dependent Propulsion of Endosomes and Lysosomes by Recruitment of N-Wasp. *J. Cell Biol.* **148**, 519–530 (2000).
42. N. C. Gauthier, P. Monzo, T. Gonzalez, A. Doye, A. Oldani, P. Gounon, V. Ricci, M. Cormont, P. Boquet, Early endosomes associated with dynamic F-actin structures are required for late trafficking of H. pylori VacA toxin. *J. Cell Biol.* **177**, 343–354 (2007).
43. R. Dong, Y. Saheki, S. Swarup, L. Lucast, J. W. Harper, P. De Camilli, Endosome-ER Contacts Control Actin Nucleation and Retromer Function through VAP-Dependent Regulation of PI4P. *Cell* **166**, 408–423 (2016).
44. M. Carnell, T. Zech, S. D. Calaminus, S. Ura, M. Hagedorn, S. A. Johnston, R. C. May, T. Soldati, L. M. Machesky, R. H. Insall, Actin polymerization driven by WASH causes V-ATPase retrieval and vesicle neutralization before exocytosis. *J. Cell Biol.* **193**, 831–839 (2011).
45. M. N. J. Seaman, The retromer complex: From Genesis to Revelations. *Trends Biochem. Sci.* **46**, 608–620 (2021).
46. R. Chakrabarti, M. Lee, H. N. Higgs, Multiple roles for actin in secretory and endocytic pathways. *Curr. Biol.* **31**, R603–R618 (2021).
47. M. J. Footer, J. W. Kerssemakers, J. A. Theriot, M. Dogterom, Direct measurement of force generation by actin filament polymerization using an optical trap. *Proc. Natl. Acad. Sci. U.S.A.* **104**, 2181–2186 (2007).
48. A. M. Gautreau, F. E. Fregoso, G. Simanov, R. Dominguez, Nucleation, stabilization, and disassembly of branched actin networks. *Trends Cell Biol.* **32**, 421–432 (2022).
49. A. Kinkhabwala, P. I. Bastiaens, Spatial aspects of intracellular information processing. *Curr. Opin. Genet. Dev.* **20**, 31–40 (2010).
50. G. R. Chichili, A. D. Westmuckett, W. Rodgers, T cell signal regulation by the actin cytoskeleton. *J. Biol. Chem.* **285**, 14737–14746 (2010).
51. M. L. Dustin, K. Choudhuri, Signaling and polarized communication across the T Cell immunological synapse. *Annu. Rev. Cell Dev. Biol.* **32**, 303–325 (2016).
52. T. D. Williams, R. Cacioppo, A. Agrotis, A. Black, H. Zhou, A. Rousseau, Actin remodelling controls proteasome homeostasis upon stress. *Nat. Cell Biol.* **24**, 1077–1087 (2022).
53. M. E. Maxson, S. Grinstein, The vacuolar-type $H^+$-ATPase at a glance - more than a proton pump. *J. Cell Sci.* **127**(Pt 23), 4987–4993 (2014).
54. J. S. King, A. Gueho, M. Hagedorn, N. Gopaldass, F. Leuba, T. Soldati, R. H. Insall, WASH is required for lysosomal recycling and efficient autophagic and phagocytic digestion. *Mol. Biol. Cell* **24**, 2714–2726 (2013).
55. E. Zavodszky, M. N. Seaman, K. Moreau, M. Jimenez-Sanchez, S. Y. Breusegem, M. E. Harbour, D. C. Rubinsztein, Mutation in VPS35 associated with Parkinson's disease impairs WASH complex association and inhibits autophagy. *Nat. Commun.* **5**, 3828 (2014).
56. B. M. Nagel, M. Bechtold, L. G. Rodriguez, S. Bogdan, Drosophila WASH is required for integrin-mediated cell adhesion, cell motility and lysosomal neutralization. *J. Cell Sci.* **130**, 344–359 (2017).
57. K. Shen, A. Choe, D. M. Sabatini, Intersubunit Crosstalk in the Rag GTPase Heterodimer Enables mTORC1 to Respond Rapidly to Amino Acid Availability. *Mol. Cell* **68**, 552–565.e8 (2017).
58. P. Poullet, S. Carpentier, E. Barillot, myProMS, a web server for management and validation of mass spectrometry-based proteomic data. *Proteomics* **7**, 2553 (2007, 2007).
59. M. The, M. J. MacCoss, W. S. Noble, L. Kall, Fast and Accurate Protein False Discovery Rates on Large-Scale Proteomics Data Sets with Percolator 3.0. *J. Am. Soc. Mass Spectrom.* **27**, 1719–1727 (2016).
60. B. Valot, O. Langella, E. Nano, M. Zivy, MassChroQ: A versatile tool for mass spectrometry quantification. *Proteomics* **11**, 3572 (2011).
61. Y. Perez-Riverol, A. Csordas, J. Bai, M. Bernal-Llinares, S. Hewapathirana, D. J. Kundu, A. Inuganti, J. Griss, G. Mayer, M. Eisenacher, E. Perez, J. Uszkoreit, J. Pfeuffer, T. Sachsenberg, S. Yilmaz, S. Tiwary, J. Cox, E. Audain, M. Walzer, A. F. Jarnuczak, T. Ternent, A. Brazma, J. A. Vizcaino, The PRIDE database and related tools and resources in 2019: Improving support for quantification data. *Nucleic Acids Res.* **47**, D442–D450 (2019).


**Acknowledgments:** We thank M.E.G. de Aruajo and L.A. Huber for discussion and advice at initial stage of this study; J. Cooper, M. Cormont, and D. Sabatini for providing constructs; S.A. Fernandes and D.-D. Angelidaki (MPI-AGE, Cologne, Germany) for technical advice and support; and members of P.C. laboratory for helpful comments during the preparation of this manuscript. We would like to acknowledge the Cell and Tissue Imaging Platform (PICT-IBiSA) and Nikon Imaging Centre at Institut Curie-CNRS of Institut Curie, members of France-Bioimaging national infrastructure supported by the French National Research Agency (ANR-10-INBS-04) for help with light microscopy. **Funding:** A.P. was supported by a grant from Association Ruban Rose (Prix Avenir 2018). A.P. and S.A. were supported by a donation from T. Paulsen, Oslo, Norway to the InvaCell project. This work was supported by grants from "Région Ile-de-France" and Fondation pour la Recherche Médicale to D.L; a grant from Fondation ARC pour la Recherche contre le Cancer (ARCPGA12019120000973_1574); a generous donation from T. Paulsen, Oslo, Norway to the InvaCell Project to P.C.; and by

institutional support from Institut Curie and Centre National pour la Recherche Scientifique to P.C. Funders had no role in study design, data collection and analysis, decision to publish, or preparation of the manuscript. **Author contributions:** Project administration and supervision: P.C. Funding acquisition: D.L. and P.C. Conceptualization: A.P., A.M.G., C.D., and P.C. Methodology: A.P., S.A.-B., P.M., D.L., and C.D. Investigation: A.P., S.A.-B., P.M., and F.D. Software: D.R. and A.-S.M. Formal analysis: A.P., S.A.-B., and V.S. Writing: A.P. and P.C. Editing: C.D. and A.M.G. **Competing interests:** The authors declare that they have no competing interests. **Data and materials availability:** All data needed to evaluate the conclusions in the paper are present in the paper and/or the Supplementary Materials. The macro for vesicle quantification is available at https://github.com/Anne-SophieMACE/EndosomalProteinDetection. Mass spectrometry data have been deposited at the ProteomeXchange Consortium (PRIDE Archive) with identifier PXD027100.

Submitted 13 July 2022
Accepted 11 August 2023
Published 13 September 2023
10.1126/sciadv.add9084

ScienceAdvances

# Codependencies of mTORC1 signaling and endolysosomal actin structures

Amulya Priya, Sandra Antoine-Bally, Anne-Sophie Macé, Pedro Monteiro, Valentin Sabatet, David Remy, Florent Dingli, Damarys Loew, Constantinos Demetriades, Alexis M. Gautreau, and Philippe Chavrier

*Sci. Adv.*, **9** (37), eadd9084.
DOI: 10.1126/sciadv.add9084